Clim Dyn
DOI 10.1007/s00382-007-0250-0

Quantifying the AMOC feedbacks during a $2\times CO_2$ stabilization experiment with land-ice melting

D. Swingedouw · P. Braconnot · P. Delecluse · E. Guilyardi · O. Marti

Received: 26 September 2006 / Accepted: 21 March 2007

Abstract The response of the Atlantic Meridional Overturning Circulation (AMOC) to an increase in atmospheric CO_2 concentration is analyzed using the IPSL-CM4 coupled ocean–atmosphere model. Two simulations are integrated for 70 years with 1%/year increase in CO_2 concentration until $2\times CO_2$, and are then stabilized for further 430 years. The first simulation takes land-ice melting into account, via a simple parameterization, which results in a strong freshwater input of about 0.13 Sv at high latitudes in a warmer climate. During this scenario, the AMOC shuts down. A second simulation does not include this land-ice melting and herein, the AMOC recovers after 200 years. This behavior shows that this model is close to an AMOC shutdown threshold under global warming conditions, due to continuous input of land-ice melting. The analysis of the origin of density changes in the Northern Hemisphere convection sites allows an identification as to the origin of the changes in the AMOC. The processes that decrease the AMOC are the reduction of surface cooling due to the reduction in the air–sea temperature gradient as the atmosphere warms and the local freshening of convection sites that results from the increase in local freshwater forcing. Two processes also control the recovery of the AMOC: the northward advection of positive salinity anomalies from the tropics and the decrease in sea-ice transport through the Fram Strait toward the convection sites. The quantification of the AMOC related feedbacks shows that the salinity related processes contribute to a strong positive feedback, while feedback related to temperature processes is negative but remains small as there is a compensation between heat transport and surface heat flux in ocean–atmosphere coupled model. We conclude that in our model, AMOC feedbacks amplify land-ice melting perturbation by 2.5.

D. Swingedouw (✉) · P. Braconnot · O. Marti
IPSL/LSCE, Orme des Merisiers, 91191 Gif-sur-Yvette, France
e-mail: didier.swingedouw@cea.fr

P. Delecluse
CNRM, 2 avenue Rapp, 75340 Paris Cedex 07, France

E. Guilyardi
IPSL/LOCEAN, Tour 45, 4 place Jussieu, 75252 Paris, France

E. Guilyardi
NCAS Climate/Walker Institute, University of Reading, Reading RG6 6BB, UK

1 Introduction

The response of the Atlantic Meridional Overturning Circulation (AMOC) to global warming (due to the increase of greenhouse gases in the atmosphere) is a matter of uncertainty for state-of-the-art coupled models. Gregory et al. (2005) used the results of 11 coupled models to show that after a quadrupling of CO_2, the AMOC decreases by between 10 and 50%. In all models, most of the weakening in AMOC is caused by changes in surface heat fluxes. Freshwater forcing changes can have either positive and negative influence on AMOC and remain thus a major source of uncertainty for future AMOC changes. These results suggest that changes in freshwater fluxes under global warming conditions can have a compensating effect to changes in surface heat fluxes for the AMOC. Addressing the specific role of salinity changes on the AMOC is therefore of paramount interest in order to reduce the uncertainty in AMOC projections for future centuries.

The AMOC response in future warming scenarios appears to be very complex and linked to several processes that affects the sites of convection. For example Latif et al. (2000) propose that the increase in tropical evaporation, associated with the increase in Atlantic-Pacific moisture transfer, stabilizes the AMOC. Wood et al. (1999) suggest that convection sites in the Labrador Sea and the Nordic Seas respond differently to global warming. In their simulations using HadCM3, the Labrador Sea convection collapses, whereas convection in the Nordic Seas is preserved, or even reinforced. In agreement, Hu et al. (2004) suggest that the Labrador Sea is very sensitive to local freshwater forcing, such that the increase in precipitation and runoff at high latitudes causes a shutdown in convection for this region. In the Nordic Seas, they note that the reduction in sea-ice cover tends to reduce the local freshwater forcing, due to reduced sea-ice melting. This effect counteracts the increase in precipitation and runoff in the North Atlantic and contributes to an increase in salinity at the sites of convection, thus maintaining convection. The balance of opposing freshwater forcings at the convection sites is therefore a key element and all the sources and sinks of freshwater should be adequately represented in models. These include: direct ocean–atmosphere evaporation minus precipitation, river and coastal runoff, sea-ice melting and brine rejection, and land-ice melting. A careful closure of the freshwater budget is of key importance in producing a reliable simulation of the AMOC changes. This is seldom the case in coupled Coupled Global Circulation Model (CGCM) and none of the models participating in the last IPCC (Cubasch et al. 2001) accounted for the land-ice melting. For current IPCC, only few models take land-ice melting into account. Impact of this melting on the AMOC is a matter of debate since studies by Fichefet et al. (2003) and Swingedouw et al. (2006) find a substantial effect of Greenland melting in transient scenario of a century, while studies of Ridley et al. (2005) and Jungclaus et al. (2006) find a negligible impact of this melting.

Another topic of considerable debate concerns the recovery of the AMOC after a shutdown or strong reduction. The possibility of multiple stable equilibriums of the AMOC as first described by Stommel (1961) has been confirmed from results of the Earth system Model of Intermediate Complexity (EMIC, Rahmstorf et al. 2005). Unfortunately, computational cost still prohibits the exploration of this concept with CGCMs. However, Vellinga et al. (2002) pointed out a stabilizing process in CGCMs that was related to gyre salinity transport (not well represented in many EMICs) and tended to assist the AMOC recovery. Stouffer et al. (2006) using a multi-model ensemble confirmed that many coupled models tend to recover after an AMOC shutdown due to a 1 Sv (1 Sv = 10^6 m^3/s) freshwater input to the sites of convection during a century. In future climate scenarios, an AMOC recovery has been observed by Stouffer and Manabe (1999) and Voss and Mikolajewicz (2001), under different atmospheric CO_2 stabilization. However the mechanisms of such recoveries are not fully understood. Moreover, the impact of land-ice melting was not accounted for, in these earlier studies, and its effect on multi-century time scale still needs to be evaluated in CGCMs.

Swingedouw et al. (2006) tackled the effects of land-ice melting in transient scenarios where the CO_2 concentration increased by 1%/year up to 4×CO_2. Using the IPSL-CM4 coupled ocean–atmosphere model, they compared two different scenarios, with and without melting from glaciers. They showed that glacial melting could accelerate the rate of AMOC weakening over 140 years. Here we evaluate the impact of land-ice melting on the recovery mechanisms over longer time scales and less extreme scenarios. To that end, new simulations were integrated for 500 years, with 430 years of stabilized CO_2 concentration at 2×CO_2. This study was designed to analyze how land-ice melting could impact the response of the AMOC and its recovery under a global warming scenario over several centuries. We are interested in evaluating how interactive land-ice melting affects AMOC recovery when CO_2 is stabilized. We develop a methodology based on an analysis of the density changes at the convection sites that allows the quantification of the processes that might be significant. Then, we evaluate the weight of each forcing and feedback on the AMOC response. We first present the set-up of the numerical experiments, and the general response of the model in scenario simulations (Sect. 2). Then the response of the AMOC during the two scenarios is analyzed (Sect. 3). Finally the forcings (Sect. 4) and feedbacks (Sect. 5) at the origin of the AMOC responses are detailed.

2 Experiments

2.1 Model description

The model used in this study is version 4 of the ''Institut Pierre Simon Laplace'' (IPSL-CM4) global atmosphere–ocean–sea-ice coupled model (Marti et al. 2005). It couples the atmosphere general circulation model LMDz to the ocean general circulation model ORCA/OPA. The LIM sea-ice model, which computes ice thermodynamics and dynamics, is also included in the ocean model and coupled to the atmosphere. Finally, the atmospheric model is coupled to the ORCHIDEE land-surface scheme.

The model grid has a horizontal resolution of 96 points in longitude and 71 points in latitude (3.7° × 2.5°) for the atmosphere and 182 points in longitude and 149 points in latitude for the ocean, corresponding to a resolution of

about 2°, with higher latitudinal resolution of 0.5° in the equatorial ocean. There are 19 vertical levels in the atmosphere and 31 levels in the ocean with the highest resolution (10 m) in the upper 150 m. The ocean and atmosphere exchange surface temperature, sea-ice cover, momentum, heat and freshwater fluxes once a day, using the OASIS coupler. River runoff and ice stream schemes close the water budget between the land and the ocean. No flux adjustments are applied and the coupling scheme ensures both global and local conservation of heat and freshwater fluxes at model interfaces.

A simple parameterization of glacier melting is included in the model (Swingedouw et al. 2006) to represent ice-sheet and mountain glaciers melting in response to climate warming. While it is based on the thermodynamic laws, it does not incorporate any dynamical mechanism. The land-ice areas are therefore fixed to the present day observed distribution. Ice is allowed to melt when the grid-box is snow free. Whenever the surface temperature is simulated to be above 0°C, the surface temperature is set to 0°C and the excess heat is used to melt the land-ice. This melting does not change the volume of ice, but only exists as an archived heat flux term. The freshwater is not directly distributed along the ice sheet, but is routed to the ocean uniformly over a wider region. Earth is divided into three latitude bands with limits at 90°S/50°S/40°N/90°N. For the northern band, the calving is sent to the Atlantic and the Nordic Seas, but not to the Pacific and the Arctic.

2.2 Numerical experiments and simulated warming

Each experiment is composed of a 500 years long control simulation (CTRL) under pre-industrial conditions (280 ppm of atmospheric CO_2 concentration, IPCC ''pictrl'' AR4). Two idealized scenario experiments were performed where the atmospheric CO_2 is increased by 1%/year up to 2×CO_2 (560 ppm reached after 70 years) and held constant for the remaining 430 years, following the CMIP2 protocol (Meehl et al. 2000). In the first scenario (WIS2), the melting from ice-sheets is included, while in the second (NIS2), it is not taken into account. Further to the analysis of Swingedouw et al. (2006) centered on the transient response up to 4×CO_2, we focus here on the AMOC response for a stabilized CO_2 (at 2×CO_2) on multi-century time scales.

After 500 years, the surface temperature at 2 m warms by 3.11 and 3.42 K globally in WIS2 and NIS2, respectively (in the high range of IPCC model warming, Forster and Taylor 2006). The atmospheric surface warming in WIS2 occurs mostly over the continent and the sea-ice (Fig. 1a) which is consistent with results reported in last and current IPCC (Cubasch et al. 2001). The climatic impact of land-ice melting can be isolated via the difference between WIS2 and NIS2 experiments (Fig. 1b, c). While we observe a relative cooling around 55°N–20°W between WIS2 and NIS2, we note an important cooling of more than 8 K in the Barents Sea. This is due to the changes in AMOC–sea-ice interactions (Swingedouw et al. 2006). We note that, in this study, cooling due to the AMOC weakening is of less importance than the warming due to greenhouse gases (in agreement with other models, Gregory et al. 2005). AMOC weakening appears to act as a damper on the warming in terms of mean temperature.

3 AMOC changes under global warming conditions

3.1 AMOC response

The AMOC index in CTRL is 10.6 Sv (Fig. 2a), which is weaker than observation-based estimates that evaluate the production of North Atlantic Deep Water to be 15 ± 2 Sv (Ganachaud and Wunsch 2000). This weakness is related to the absence of convection in the Labrador Sea, associated to a freshwater forcing bias (Swingedouw et al. 2007). In WIS2, the AMOC weakens to around 3.3 Sv after 500 years. In NIS2, the AMOC index decreases over the first 100 years to about 8 Sv and then recovers to the CTRL value at around year 200. These differences in AMOC are associated with changes in the regions of deep water formation. Figure 3 shows the annual maximum of the mixed layer depth, which is a proxy of the ocean convection in these regions. Compared to CTRL, convection is reduced over the whole North Atlantic in WIS2, while in NIS2 it is reinforced in the Nordic Seas, in agreement with the studies of Wood et al. (1999) and Hu et al. (2003), and weakened in the Irminger Sea.

The difference in the response of the AMOC is related to differences in the freshwater forcing (mainly the melting of Greenland ice-sheet). The warming over Greenland reaches 3.8 K in WIS2 and contributes to melting of ice-sheet. Meltwater is not allowed to impact the ocean in the NIS2 case. There is thus a difference of 0.13 Sv in freshwater forcing uniformly distributed in the Atlantic (north of 40°N) and Nordic Seas (south of 80°N) between the two scenarios after 200 years. The melting elsewhere is lower than 0.02 Sv after 500 years so that we make the assumption that its effect is negligible compared to the Greenland melting. After 500 years, the integrated meltwater flux in the north is equivalent to the melting of more than half of the Greenland ice-sheet. This is an extreme scenario, not supported by the results of a three dimension dynamical ice-sheet model forced by global warming conditions (Parizek and Alley 2004). That said, such a forcing could have been observed during the last interglacial period (Overpeck et al. 2006). The extreme melting

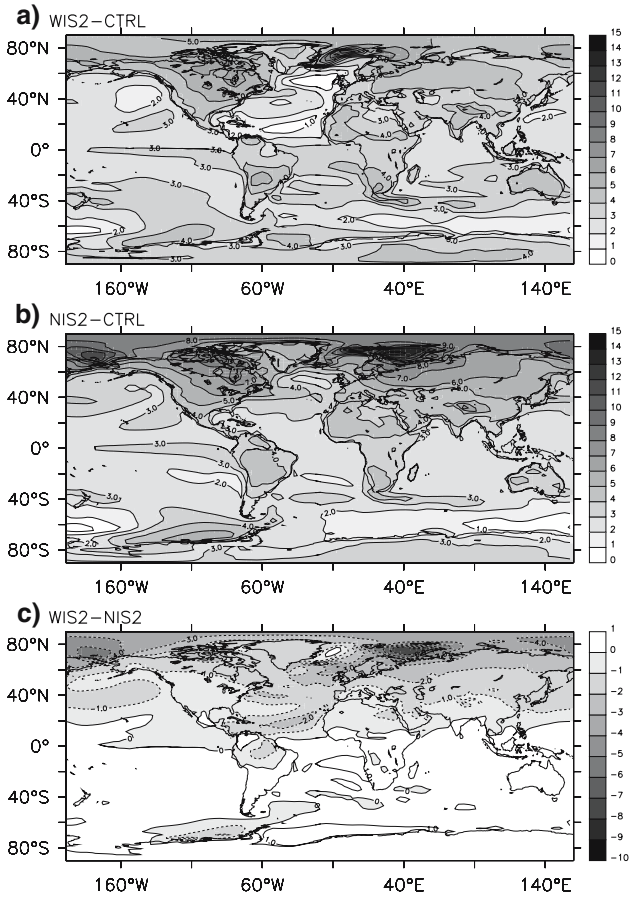

Fig. 1 Difference in air temperature at 2 m averaged over the last 30 years of the experiments, **a** WIS2-CTRL, **b** NIS2-CTRL, **c** WIS2-NIS2. The contour interval is 1 K

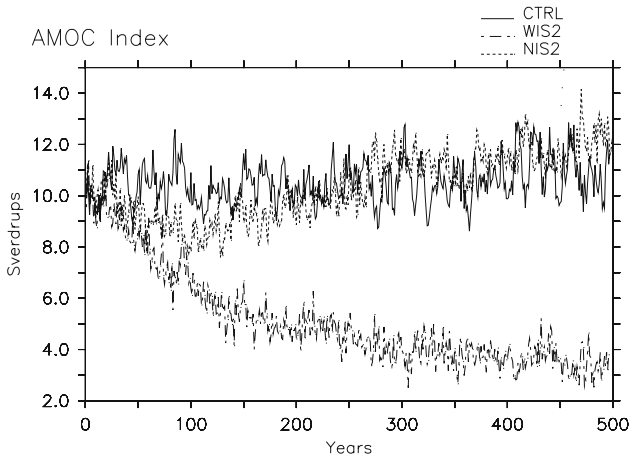

Fig. 2 Evolution for the three experiments of the AMOC index, defined as the maximum of the vertical streamfunction between 500 and 5,000 m in the Atlantic

simulated in WIS2 is partly due to the crude parameterization of the ice-sheet melting with a fixed ice-sheet extension (Swingedouw et al. 2006) and that does not consider refreezing processes nor the change in ice-sheet geometry. Nevertheless, since there are large uncertainties associated with ice-sheet melting, our scenarios highlight an important feature of the ice-sheet and ocean interaction by spanning the range of possible impacts. In one case (NIS2) the AMOC recovers and in the other (WIS2), the AMOC greatly weakens.

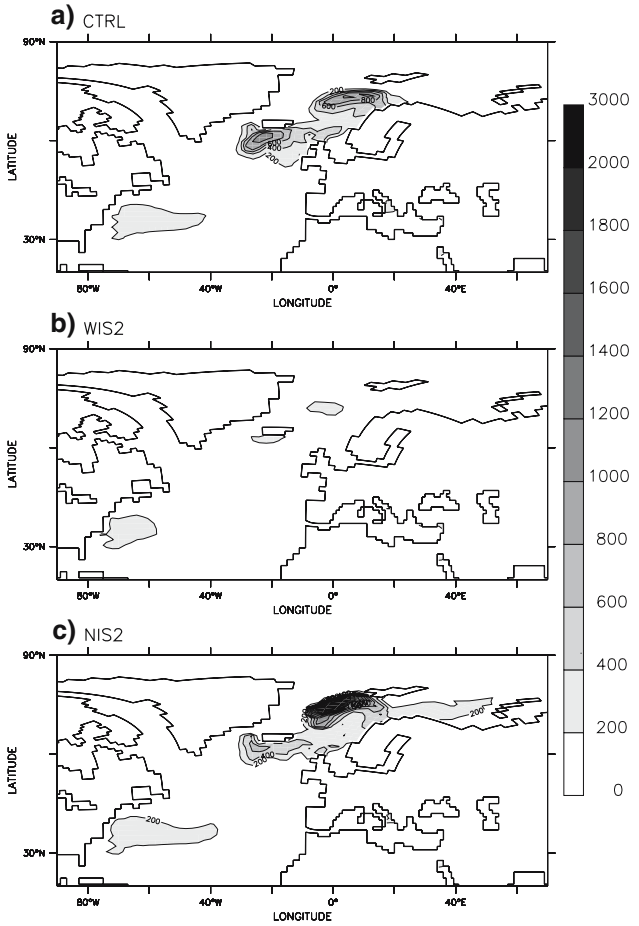

Fig. 3 Annual maximum mixed layer depth (in m) averaged over the last 30 years of simulation for **a** CTRL, **b** WIS2 and **c** NIS2

3.2 AMOC and stratification in the convection sites

The strength of the AMOC can be assessed by using several oceanic characteristics (Vellinga et al. 2004). Following the assumptions of Hughes and Weaver (1994), Thorpe et al. (2001) have shown that the AMOC is highly correlated with the steric height gradient between 35°S and 60°N in the HadCM3 ocean–atmosphere model. This is in agreement with the Stommel box model (Stommel 1961), where AMOC strength was related to a north–south density gradient. However, as noted by Straub (1996), the parameterization of the transport in the Stommel box model is inconsistent with the Stommel-Arons model (1960) where

the AMOC transport is calculated, given a rate of deep water formation. This suggests that considering the changes in the rate of deep water formation is a good indicator of changes in the AMOC. As convection produces large amounts of deep water through mixing and cooling, the amount of deep water formation is related to the intensity of convection in the Nordic Seas. For instance, if a halocline develops at the surface, cooling by the atmosphere is limited to the upper part of the ocean water column, which restricts deep water formation. In a transient phase (less than a millennial time scale), a density anomaly in the convection sites is strongly correlated with depth averaged density (Delworth et al. 1993), and is therefore a good proxy for the AMOC amplitude as verified for IPSL-CM4 by Swingedouw et al. (2007).

To further demonstrate this relationship, we define in the model a region covering all convection sites (Fig. 4a) and we represent in Fig. 4b the difference in AMOC index as a function of the difference in potential density averaged at the convection sites region over the whole depth between the scenarios and CTRL for the 500 years of simulation. The correlation between density anomaly in the convection sites ($\Delta\ \rho$, kg/m^3) and AMOC index changes (ΔAMOC, Sv) is 0.98. We therefore deduce the following relation:

$$\Delta\mathrm{AMOC} \approx \gamma \Delta\rho \quad (1)$$

where γ = 23 Sv·kg^{-1}·m^3 . Other regions at different latitudes have been considered in order to verify that the high correlation is not due to transient response effects. No other regions exhibits as good a correlation with the AMOC index (not shown). In the following, we use this correlation between density in the convection sites and AMOC index to examine which changes in density forcing and which mechanisms have perturbed the AMOC in the WIS2 and NIS2 experiments.

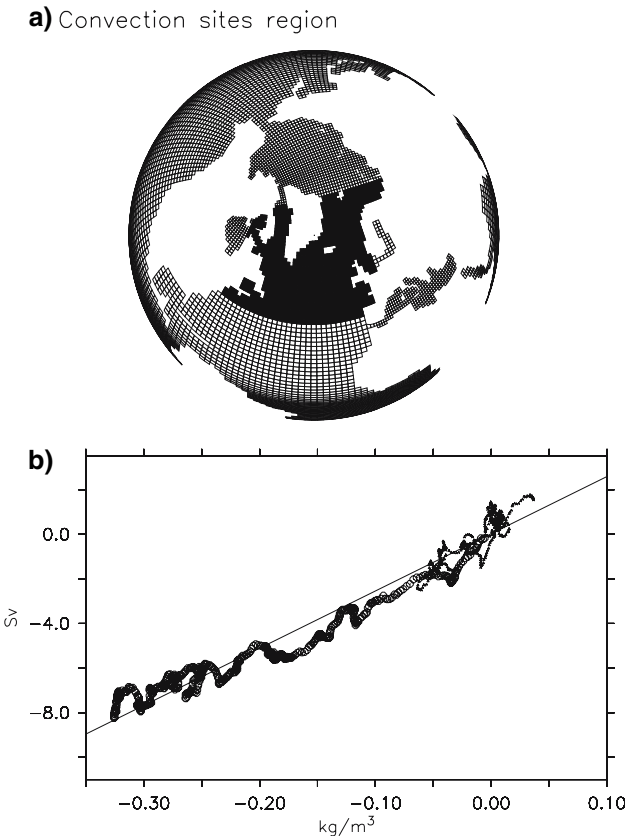

Fig. 4 **a** Region (in black) used to average the different terms in the convection sites. **b** Correlation between the anomalies of WIS2 (*circle*) and NIS (*cross*) minus CTRL, for the AMOC and the averaged density in the convection sites. A 17 years smoothing, which corresponds to the period of the maximum of the variability frequency, is applied. The correlation is 0.98

3.3 Thermal versus haline forcing

Temperature and salinity both contribute to any change in density. In order to distinguish their respective contributions, we linearize the density equation. Thus we express changes in AMOC as a function of thermal and haline changes via the following equation:

$$\Delta\mathrm{AMOC} \approx \gamma(\beta\Delta S + \alpha\Delta T) \quad (2)$$

where ΔS and ΔT represents the salinity and the temperature anomalies in the convection sites when compared to CTRL. α and β are the thermal and haline expansion, respectively. They are function of T and S and are calculated for each grid box. By averaging over depth at the convection sites region, we obtain a thermal and haline contribution. The time evolution of these thermal and haline contributions are shown in Fig. 5 for both scenarios.

In NIS2, where land-ice melting is not modeled, density decreases for the first 100 years (Fig. 5a), and then increases for the rest of the simulation. The haline contribution to density change is positive and increases with time to reach 0.39 kg/m^3 after 500 years. The thermal contribution decreases during the entire simulation, reaching –0.36 kg/m^3 after 500 years. After 100 years, the balance of these two opposing effects is dominated by the positive haline density anomaly, which is therefore the origin of the AMOC recovery in NIS2. In WIS2, where the land-ice melting is taken into account, the density anomaly decreases and is negative for the whole simulation. Both thermal and haline contributions have a negative impact reaching –0.16 kg/m^3 for both components after 500 years, and cause a weakening in the AMOC.

These two simulations show that ocean temperature warming tends to weaken the AMOC, while the salinity influence can be either positive (NIS2) or negative (WIS2)

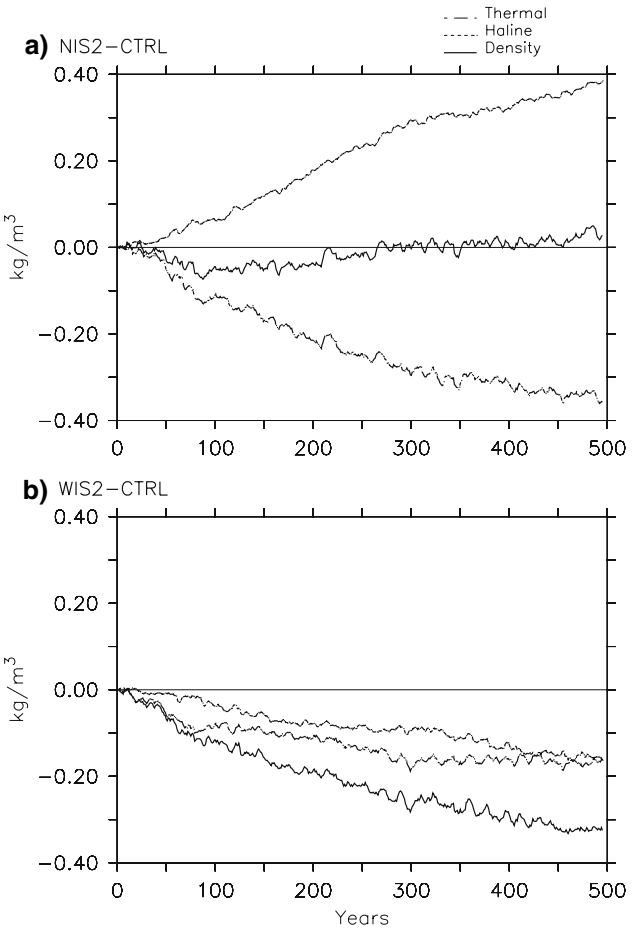

Fig. 5 Density anomaly averaged over the convection sites (*continuous line*), with its thermal contribution (*semi-dotted line*), and its haline contribution (*dotted line*). **a** NIS2-CTRL, **b** WIS2-CTRL

and is thus a driver of either AMOC recovery or weakening. In order to assess which forcings are at the origin of these different thermal and haline contributions, we further decompose the density balance in regions of convection.

4 Forcings and mechanisms affecting the AMOC

4.1 Change in density balance in the convection sites

The thermal and haline contribution to density either result from changes in local surface fluxes or from changes in oceanic transport. Thus we expand the density change over the whole depth of the ocean in terms of meridional transport change ($\Delta\ \rho_{\text{transport}}$) and surface flux change ($\Delta\ \rho_{\text{flux}}$), related to salinity ($\Delta\ \rho^S$) and temperature ($\Delta\ \rho^T$). The other terms ($\Delta\ \rho_{\text{OT}}$, diffusion, zonal transport change) are brought together. This results in the following:

$$\begin{aligned}\Delta\rho = {} & \Delta\rho^S_{\text{transport}} + \Delta\rho^S_{\text{flux}} + \Delta\rho^S_{\text{OT}} \\ & + \Delta\rho^T_{\text{transport}} + \Delta\rho^T_{\text{flux}} + \Delta\rho^T_{\text{OT}}\end{aligned} \tag{3}$$

The different terms are computed using the equation of the tracer conservation in the model, integrated in depth over the convection sites box (Fig. 4.a). This equation, for a tracer Θ (salinity or the temperature), is:

$$\underbrace{\iiint_{\Omega} \frac{\partial\Theta}{\partial t} \mathrm{d}v}_{\text{Tracer evolution}} = \underbrace{-\iint_{\delta\Omega_l} \vec{V_h}\ \Theta\ \vec{\mathrm{d}\sigma}}_{\text{Horizontal advection}} + \underbrace{\iint_{\delta\Omega_l} \vec{v}\ .\ \vec{\nabla}\ \Theta \mathrm{d}\sigma}_{\text{Diffusion}}$$

$$+ \underbrace{\iint_{z=\eta} (\varepsilon - w_s)\Theta \mathrm{d}\sigma}_{\text{Surface flux}} \tag{4}$$

where Ω is the convection sites region, $\delta\Omega_l$ is the lateral boundaries, and η is the free surface. V_h is the horizontal speed, $\vec{v}$ is the diffusion tensor, w_s is the vertical velocity at the surface, and $\varepsilon\Theta = \frac{Q_{\text{net}}}{\rho_0 C_p}$ for temperature, where Q_{net} is the net surface heat flux and $\rho_0 C_p$ is the heat flux capacity, and ε = E-P-R for salinity, where E is the evaporation, P the precipitation and R the runoff.

In Fig. 6 we present the integration over 500 years of these different terms for the two experiments (minus CTRL). All terms are multiplied by α and β and then averaged on the convection sites box in order to be expressed in density units (kg/m^3) for a quantitative comparison of their contributions to density. A positive (negative) value corresponds to an increase (decrease) in density, and thus of AMOC. The different terms in both scenarios have the same sign, but their sum is of opposite sign (Fig. 6). Surface salinity forcing and heat transport tend to increase the density whereas surface temperature forcing and salinity transport reduce it.

In NIS2, the surface salinity forcing is the dominant positive term and is larger than the most dominant negative

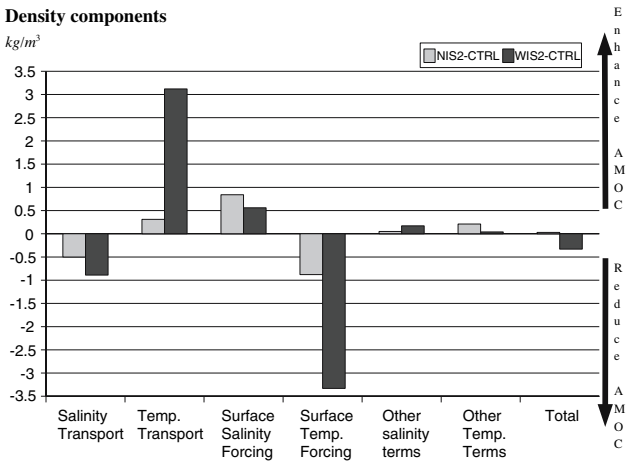

Fig. 6 Magnitude of the different terms contributing to the density changes in the convection sites region, integrated on the 500 years of the experiments and expressed in kg/m^3. *Black bars* stands for the difference WIS2-CTRL, and *light grey bars* for NIS2-CTRL

term, which is the surface heat flux change $\Delta\ \rho^{T}_{\mathrm{flux}}$. In WIS2, all terms have a larger magnitude than in NIS2. The negative effect of surface temperature forcing and salinity transport dominate the positive surface salinity forcing and heat transport, resulting in a reduction in density.

4.2 Changes in surface forcing

In both experiments the thermal surface forcing reduces surface density at the convection sites, which means that the heat flux changes tend to warm the ocean. The different components of the thermal surface forcing are plotted in Fig. 7a. In both scenarios, they have the same sign except

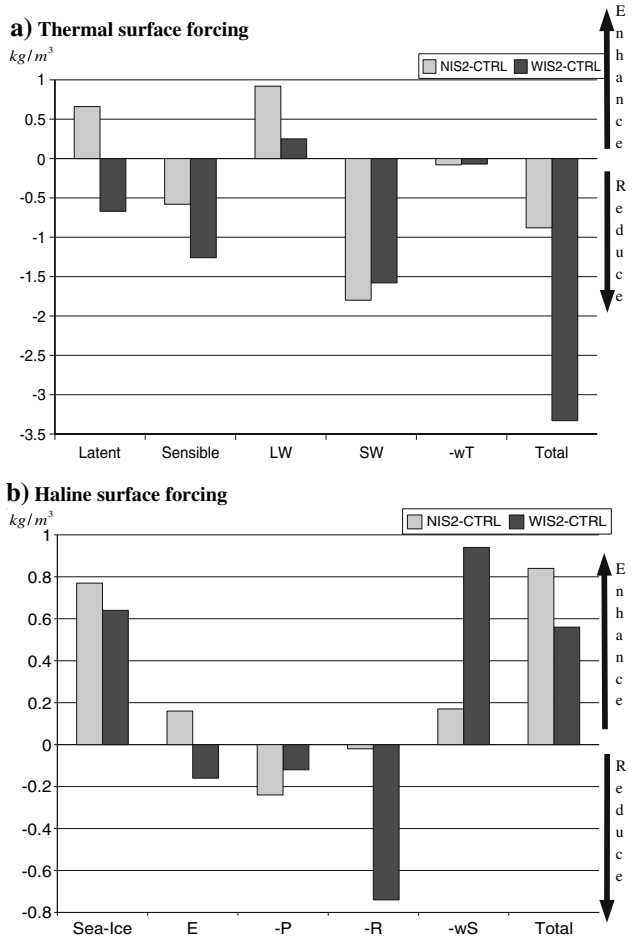

Fig. 7 Magnitude of the different terms contributing to density surface forcing anomaly between scenarios and CTRL simulation, expressed in density units (kg/m^3) and integrated over 500 years. **a** For surface temperature forcing, it is decomposed in latent heat flux (Latent), sensible heat flux (Sensible), long wave flux (LW), short wave flux (SW), free surface adjustment (–wT) and the total of these five terms is given in the last column. In *black* is the difference WIS2-CTRL, and in *light grey* the difference NIS2-CTRL. **b** For salinity surface forcing, it is decomposed in ice melting contribution (Sea-Ice), evaporation contribution (E), precipitation contribution (-P), runoff contribution (-R) and free surface adjustment (–wS). Note the different vertical scale for **a** and **b**

for the latent heat flux anomaly. The short wave term is negative, which means that more solar flux penetrates the ocean, resulting in a warming, due to the reduction of sea-ice cover in summer. The long wave term is positive, and reflects the fact that a warmer ocean emits more long wave radiation, which tends to cool it. This term is however less important than the short wave negative term. The sensible heat flux term is negative which means that it tends to warm the surface in both simulation. The latent heat flux term is positive in NIS2 and negative in WIS2 and has thus a different contribution to the net heat flux. These last two terms depend on the wind stress, the stability of the boundary layer, the temperature gradient between the ocean and the atmosphere, and the relative humidity for the latent heat flux, so that an explanation of the changes is not straightforward.

In both experiments, the change in surface freshwater forcing ($\Delta\ \rho^{S}_{\mathrm{flux}}$) is positive (Fig. 6) and assists AMOC recovery. In Fig. 7.b, the balance in surface freshwater forcing in density is decomposed into evaporation (E), precipitation (-P), runoff (-R), sea-ice freshwater flux and changes in free surface flux (–wS) integrated in time across the convection sites. The last term (–wS) is affected by the mass input of E-P-R, but not by sea-ice, as sea-ice melting does not lead to any surface elevation. Consequently, –wS damps the effect of E-P-R by more than 85% in both scenarios. The sea-ice changes are positive and play an important role in the surface salinity forcing in both scenarios, as since the net freshwater forcing is positive.

Following the difference in the latent heat flux, evaporation anomaly is positive for NIS2 and negative for WIS2. In NIS2, the terms -P and -R show a small decrease for the global freshwater balance, associated with an intensification of only 7% in the hydrological cycle (global precipitation rate) after 500 years, which is of the same order in both scenarios (not shown). The difference between NIS2 and WIS2 in terms of glacial melting forcing appears in the term -R. The magnitude of this term is 2.6 time more important than the sum of negative values of E and -P in WIS2. Although it seems logical that sea-ice melting will increase in a warmer climate, during the transient response, and will decrease salinity at the convection sites, the effect of sea-ice melting is positive in both simulation and has a large magnitude. This effect is further investigated in the following through sea-ice dynamics analysis.

The sea-ice contribution to density in the convection sites results from a direct local effect and sea-ice transport mostly through the Fram Strait (Fig. 8a). The local effect is melting in summer, and brine rejection in winter. A balance of these two freshwater terms expressed in Sv (Fig. 8b) shows that in CTRL the local contribution is negative by –0.06 Sv, illustrating that the convection sites are dominated by brine rejection. However, the total contribution

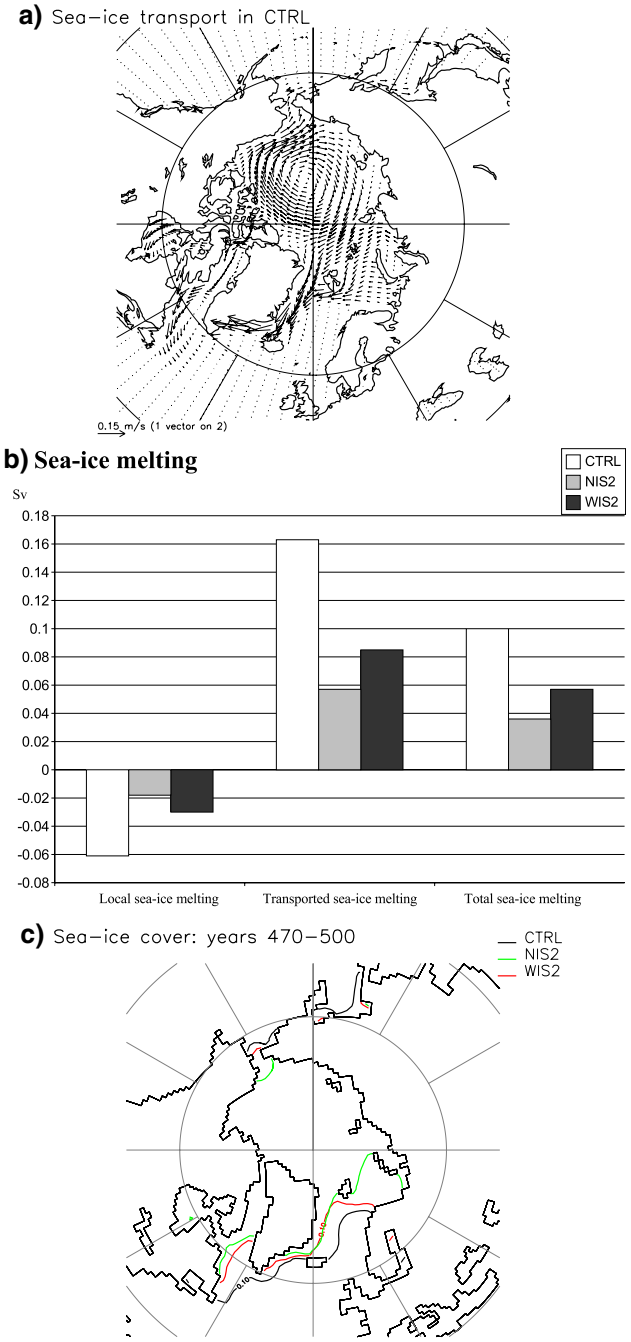

Fig. 8 **a** Ice transport in the Arctic as simulated in CTRL, **b** Total sea-ice melting in the convection sites and its two components: local sea-ice melting and transported sea-ice melting, for CTRL (*white*), WIS2 (*black*) and NIS2 (*grey*). **c** Sea-ice cover averaged over 30 years at the end of the simulation. The *black line* represents CTRL, the *dark grey* (red) line WIS2 and the *light grey* (green) line NIS2

due to sea-ice melting is +0.1 Sv, due to the +0.16 Sv import of sea-ice through the Fram Strait. In the two experiments, the negative sea-ice melting anomaly in the convection sites (–0.06 Sv in NIS2, –0.04 Sv in WIS2, Fig. 8c) results from a diminution of the Fram Strait transport (–0.1 Sv in NIS2, –0.07 Sv in WIS2). This effect is only partially balanced by a reduction in the direct sea-ice brine rejection (+0.04 Sv in NIS2, +0.03 Sv in WIS2) due to a decline in the sea-ice cover. Thus, the positive anomaly $\Delta\ \rho^{S}_{\mathrm{flux}}$ in Fig. 6 is mostly associated with a decrease in sea-ice export through the Fram Strait.

4.3 Tracer transport changes

We now focus on the thermal and haline transport changes after 500 years in both scenarios. We consider the northern and southern borders of the box which dominate the advection balance (advection from the Baltic Sea and Hudson Bay represents less than 1% for the balance and is thus negligible). To isolate the effect of circulation changes from the effect of changes in the tracer fields, we use the following decomposition: $\Theta = \Delta\ \Theta + \ \Theta_{\mathrm{ctrl}}$ where $\Delta\ \Theta$ represents the tracer anomaly compared to CTRL, and Θ_{ctrl} is the tracer value of CTRL, and similarly for the meridional northward velocity: $V = \Delta V + \ V_{\mathrm{ctrl}}$. This results in the following decomposition for the tracer transport:

$$\Delta\rho^{\Theta}_{\mathrm{transport}} = -\Delta(V\Theta) = -V_{\mathrm{ctrl}}\Delta\Theta - \Delta V\Theta_{\mathrm{ctrl}} - \Delta V\Delta\Theta \tag{5}$$

As above, all terms are averaged over depth along the boundaries of the convection sites and are expressed in density unit through scaling by thermal (α) or haline (β) expansion. The total anomaly of the tracer transport Θ in reference to CTRL is $-\Delta\ (V\Theta) = \Delta\ \rho^{\Theta}_{\mathrm{transport}}$. Anomalies are equal to either $\Delta\ \rho^{S}_{\mathrm{transport}}$ or $\Delta\ \rho^{T}_{\mathrm{transport}}$ if Θ is the salinity or the temperature, respectively. The transport of tracer anomalies is $-V_{\mathrm{ctrl}}\ \Delta\ \Theta$. The transport of the tracer field due to the anomaly in meridional velocity is $-\Delta V\ \Theta_{\mathrm{ctrl}}$. The non linear transport is $-\Delta V\ \Delta\ \Theta$.

All terms for temperature and salinity are shown in Fig. 9. In NIS2, the sum of all contributions reduces density at the convection sites. However, the dominant term in magnitude is $-V_{\mathrm{ctrl}}\Delta S$ (which is positive) and is associated with a change in the salinity field and not a change in circulation. The terms $-\Delta V\ T_{\mathrm{ctrl}}$ and $-\Delta V\ \Delta T$ are also positive but have smaller magnitudes. All the other terms are negative and result in a negative total balance. In WIS2, the total balance is positive and mostly associated with the transport of heat by the circulation anomaly ($-\Delta V\ T_{\mathrm{ctrl}}$) and the transport of the salinity anomalies ($-V_{\mathrm{ctrl}}\ \Delta S$). They are damped by the negative term $-\Delta V\ S_{\mathrm{ctrl}}$. While the magnitude of the transport terms are stronger in WIS2 than in NIS2, we note that the term $-V_{\mathrm{ctrl}}\Delta S$ has nearly the same amplitude for both experiments. This term represents the transport of salinity anomalies from remote areas as this is mostly related to gyre transport (not shown), it is thus only slightly affected by AMOC changes. The values of the

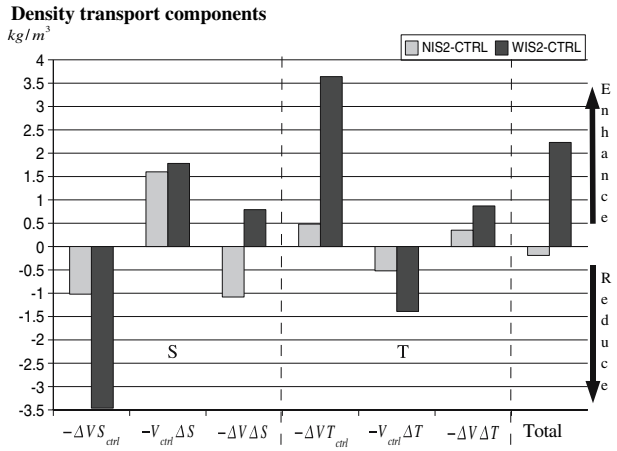

Fig. 9 Decomposition of the salinity and temperature transport into anomaly of transport ($\Delta V\ S_{ctrl}$ and $\Delta V\ T_{ctrl}$), transport of tracer anomaly ($V_{ctrl}\ \Delta S$ and $V_{ctrl}\ \Delta T$) and non linear terms ($\Delta V\ \Delta S$ and $\Delta V\ \Delta T$). The last column gives the total effect of these transport terms on the density of the convection sites. *S* and *T* stand for the salinity and temperature related columns, respectively, separated by a *dotted line*

contribution to the density balance at the convection sites are summarized in Table 1 for NIS2 experiment and in Table 2 for WIS2 experiment.

4.4 Transport of salinity anomaly: origin and timing

Since the transport of salinity anomalies ($-V_{ctrl}\Delta S$) appears as an important recovery mechanism in our two simulations, its origins are of interest. In both scenarios the temperature increases and is associated with a 7% increase in global evaporation after 500 years. The latitudinal section of salinity anomalies in NIS2 compared to CTRL is shown in Fig. 10a and illustrates a positive salinity anomaly between 40°S and 40°N. Poleward of 40°N, the positive anomalies of salinity are located in subsurface, while surface water salinity are dominated by local freshening due to the increase in freshwater forcing.

Figure 10b describes how these surface anomalies evolves with latitude as a function of time. Salinity anomalies, originating from low latitudes, develop and reach the latitude of the convection sites (50°N) after 100 years in NIS2 experiment. This delay is comparable to the lag observed for the AMOC recovery in this experiment, and might explain it. This suggests that the AMOC firstly weakens because of the direct warming at high latitudes. This effect is damped by the decrease of sea-ice transport through Fram Strait, with a short lag (not shown). The AMOC then slowly recovers after 100 years due to the northward advection of salinity anomalies.

Figure 11 shows the atmospheric moisture transport for CTRL and difference with NIS2. We note that in CTRL the Atlantic basin mostly exports moisture towards the Pacific at the equatorial latitude (Fig. 11a). This explains why the E-P-R budget over the Atlantic is positive in CTRL. The origin of the increase in the E-P-R balance in NIS2 is related to changes in moisture transport. The export of freshwater from the Atlantic increases, due to an increase in the Atlantic-Pacific transfer at the equator, as well as an increase in the transport to the Antarctic basin (Fig. 11b). The exchange of moisture between the Atlantic and the Pacific via atmospheric circulation increases, but is not related to a ''permanent'' El Nino (Guilyardi 2006), contrary to the Latif et al. (2000) mechanism.

The balance of freshwater forcing over the entire Atlantic varies in the experiments. It is –0.26 Sv in CTRL and increases up to –0.39 Sv after 500 years in NIS2. In WIS2, the balance remains of –0.26 Sv as in CTRL. Overall, this result

Table 1 Summary of the magnitude in kg/m^3 of the different terms that compose the density balance in the convection sites for the experiments NIS2-CTRL

Salinity: $\beta\ \Delta S$ = 0.39								
Surface forcing = 0.84					Salinity transport = –0.50			Other terms
Ice	E	-P	-R	–wS	$-\Delta V\ S_{ctrl}$	$-V_{ctrl}\ \Delta S$	$-\Delta V\ \Delta S$	
0.77	0.16	–0.24	–0.02	0.17	–1.02	1.60	–1.08	0.05
Temperature: $\alpha\ \Delta T$ = –0.36								
Surface forcing = –0.88					Temperature transport = 0.31			Other terms
Lat	Sens	LW	SW	–wT	$-\Delta V\ T_{ctrl}$	$-V_{ctrl}\ \Delta T$	$-\Delta V\ \Delta T$	
0.66	–0.58	0.92	–1.80	–0.08	0.48	–0.52	0.35	0.21

The decomposition follows Eqs. 3 and 5. The terms Ice, E, -P, -R, –wS correspond to the surface density forcing associated to sea-ice, evaporation, precipitation, runoff, and free surface adjustment effect on salinity respectively, following notation of Eq. 4, and integrated over the surface and in time. The terms Lat, Sens, LW, SW, –wT correspond to the surface density forcing associated to latent, sensible long wave, short wave and free surface adjustment effect on temperature respectively. The different terms of salinity transport follow notation of Eq. 5

Table 2 Same as Table 1 but for WIS2-CTRL

Salinity: $\beta\,\Delta S$ = –0.16								
Surface forcing = 0.56					Salinity transport = –0.89			Other terms
Ice	E	-P	-R	–wS	$-\Delta V\,S_{ctrl}$	$-V_{ctrl}\,\Delta S$	$-\Delta V\,\Delta S$	
0.64	–0.16	–0.12	–0.74	0.94	–3.46	1.78	0.79	0.17
Temperature: $\alpha\,\Delta T$ = –0.16								
Surface forcing = –3.33					Temperature transport = 3.12			Other terms
Lat	Sens	LW	SW	–wT	$-\Delta V\,T_{ctrl}$	$-V_{ctrl}\,\Delta T$	$-\Delta V\,\Delta T$	
–0.67	–1.26	0.25	–1.58	–0.07	3.64	–1.39	0.87	0.05

The land-ice melting is included in the term -*R*

illustrates the fact that under an identical global freshwater forcing of the whole Atlantic (CTRL and WIS2), the AMOC can exhibit different behavior (Gregory et al. 2003). Thus the AMOC is most sensitive to the freshwater balance around its convection sites (Rahmstorf 1996).

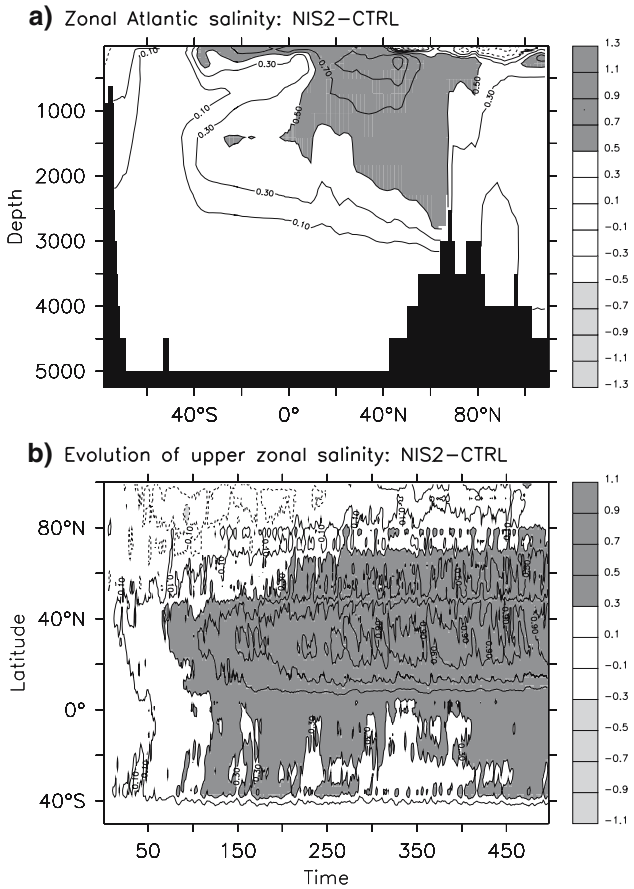

Fig. 10 Zonal mean difference between NIS2 and CTRL of Atlantic salinity plotted as a function of latitude and **a** depth, averaged over years 470 to 500, and **b** time averaged over the top 500 m. The contour interval is 0.2 PSU

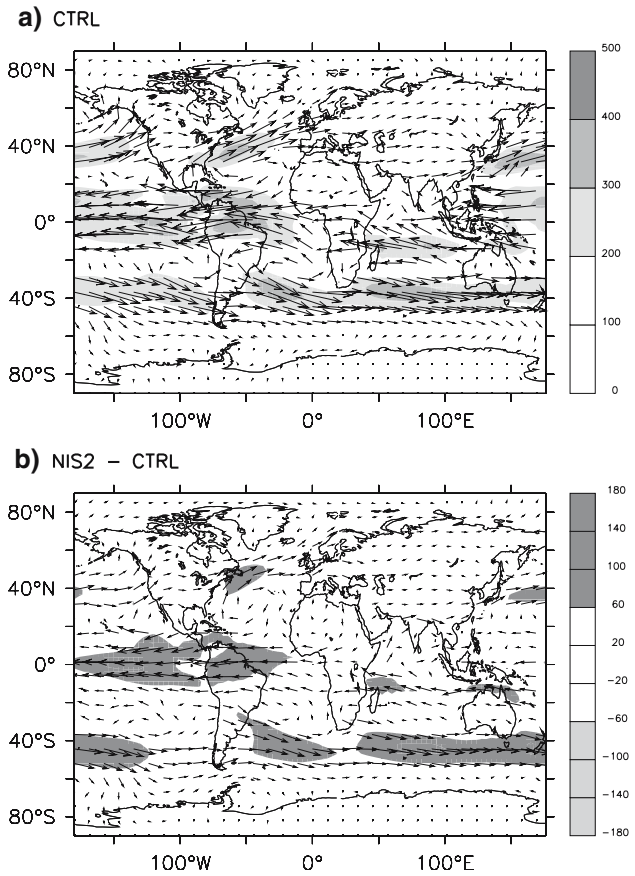

Fig. 11 Moisture transport in kg/m^2 s averaged over years 470 to 500, **a** CTRL, **b** difference between NIS2 and CTRL

5 AMOC feedbacks

The difference in the density budget between WIS2 and NIS2 at the convection sites allows us to examine the significance of the potential feedbacks (transport, surface fluxes, ...) of the AMOC system.

5.1 Feedback factor definition

The exact evaluation of a particular feedback requires a specific sensitivity experiment where the analyzed feedback loop is the only component that can vary in the system (the other components being kept equal). This type of analysis requires a large amount of computer resources for a CGCM. Here we utilize our two scenarios with different AMOC intensity. We consider that the input perturbation of the AMOC system is associated to the freshwater input due to Greenland melting, and the output is the density difference between WIS2 and NIS2 at the sites of convection ($\Delta\rho$ = –0.36 kg/m^3). In the following, we only consider WIS2 and NIS2 and Δ now refers to the difference between them. The input to the AMOC system is the effective density anomaly $\Delta\,\rho_0$ at the convection sites. $\Delta\,\rho_0$ is associated with land-ice melting and is adjusted by the dynamical free surface. We neglect the feedback effect in E-P-R balance between the scenarios since they are small (cf. Sect. 2). Thus, we define $\Delta\rho_0 = \Delta(\text{E-P-R} - w_s)S = -0.14\,kg/m^3$. Following Eq. 3 we can write:

$$\frac{\Delta\rho}{\Delta\rho_0} = \frac{1}{1 - \sum_\xi \frac{\Delta\rho_\xi}{\Delta\rho}} \tag{6}$$

where ξ represents the term considered, related to salinity transport for example. This form is a classic definition of feedbacks used in electronics and in climate science from the pioneering work of Hansen (1984). If we define $\lambda_\xi = \Delta\,\rho_\xi/\Delta\,\rho$, λ_ξ represents the feedback factor of the system. If λ_ξ is positive (negative), the feedback considered is positive (negative).

5.2 Feedback factor quantification

The feedback factors (λ_ξ) estimated for the different processes considered in this study are presented in Table 3. Following Eq. 6, we first note that the dynamical gain $\Delta\,\rho/\Delta\,\rho_0$ of the system is equal to 2.5, which is higher than 1. This means that the AMOC system tends to amplify the initial density anomaly. This is due to the positive feedback factor λ_S related to salinity (which is higher than the negative feedback factor λ_T related to temperature, Table 3). In the following, we decompose these two feedback factors following the methodology developed in Sect. 1.

The feedback factor associated with salinity transport (λ_{ST}) dominates the other salinity factors. It is the sum of the feedback factors associated with the anomaly in velocity transport ($\lambda_{\Delta V S_{ctrl}}$), the non linear salinity transport ($\lambda_{\Delta V\ \Delta S}$) and the transport of salinity anomalies ($\lambda_{V_{ctrl}\Delta S}$). The last two terms are negative while the first one is positive and explains why λ_{ST} is positive too. Thus, if the feedback associated to salinity is positive, it is mostly because of the salinity transport strength, which is associated with changes in velocity. Stommel (1961) first discussed this feedback as being very important for the AMOC dynamics. He described it as follows: a weakening of the AMOC weakens the meridional ocean velocity, which weakens the salinity transport from the tropics toward the convection sites, which further weakens the AMOC. Table 3 also confirms the existence of a weak positive feedback associated with sea-ice melting, described by Yang and Neelin (1993): when the AMOC increases, the atmospheric temperature of the Northern Hemisphere increases and melts the Arctic sea-ice, thus reducing the import of sea-ice at the convection sites through the Fram Strait. This increases the salinity in the convection sites, and enhances the AMOC.

The feedback factor associated with the heat transport (λ_{HT}) dominates the feedback factor associated with temperature (λ_T). The heat transport feedback is negative because of the anomaly in velocity transport ($\lambda_{\Delta V T_{ctrl}}$), as the other heat transport terms are smaller. This classical heat transport negative feedback was already described by Stommel (1961): a weakening of the AMOC weakens the meridional ocean velocity, which weakens the heat transport from the tropics toward the convection sites, leading to a cooling. This tends to assist AMOC recovery. Our analysis shows that this heat transport feedback (λ_{HT}) is damped by the strong positive feedback factor (λ_{SHF}) associated with the surface heat flux. It is explained as follows: an increase in the AMOC increases the surface temperature at the convection sites, thereby increases the heat flux cooling by the atmosphere. This tends to reduce

Table 3 Feedback factor decomposition

Salinity: λ_S = 1.13					Temperature: λ_T = –0.53				
Freshwater	Transport: λ_{ST} = 1.09			Other	Heat Flux	Transport: λ_{HT} = –7.80			Other
$\lambda_{SSF} = \lambda_{Ice}$	$\lambda_{\Delta V S_{ctrl}}$	$\lambda_{V_{ctrl}\Delta S}$	$\lambda_{\Delta V\ \Delta S}$	λ_{OTS}	λ_{SHF}	$\lambda_{\Delta V T_{ctrl}}$	$\lambda_{V_{ctrl}\Delta T}$	$\lambda_{\Delta V\ \Delta T}$	λ_{OTT}
0.37	6.78	–0.49	–5.20	–0.33	6.81	–8.78	2.42	–1.44	0.46

Each term is calculated as $\lambda_\xi = \Delta\rho_\xi/\Delta\rho$ where $\Delta\,\rho_\xi$ represents the term from the decomposition of Tables 1 and 2, and Δ refers now to the difference between the two scenarios WIS2-NIS2. Note that the feedback factor related to surface freshwater fluxes (λ_{SSF}) is equal in this analysis to sea-ice's one (λ_{Ice})

the temperature at the convection sites, which enhances the AMOC. This feedback is only found in a coupled system, and will be absent in ocean only models. The feedback factor λ_T is consequently small compared to λ_S, because two opposing factors associated with heat transport and heat flux compensate for each other. Thus it is the salinity positive feedback that explains the high sensitivity of the AMOC system.

6 Discussion and conclusions

In this study we have extended the experiments of Swingedouw et al. (2006) analyzing the impact of land-ice melting on the AMOC under global warming condition. From coupled ocean–atmosphere experiments in which the atmospheric concentration in CO_2 is increased during 70 years and stabilized at 2×CO_2 for 430 years, we have shown that the AMOC response to global warming in the IPSL-CM4 coupled model is very sensitive to the assumption made about the fate of the meltwater from Greenland. In this model, the parameterized melting of glaciers and ice-sheets results in a strong weakening in the AMOC. The AMOC recovers in two centuries if this melting is not included in the surface water flux. We stress the importance of the melting of Greenland's glaciers on the AMOC, over multi-century time scales. Thus, we argue that land-ice models need to be improved and incorporated into CGCMs.

In the perturbed simulations, surface forcing changes are global and affect the thermal as well as the haline forcing distribution. Thus, a careful analysis is necessary in order to understand which processes are of importance in explaining changes in the AMOC. A methodology, based on the high correlation between AMOC variations and potential density changes averaged over the North Atlantic convection sites, was developed to evaluate the relative contribution of the different forcing terms on the AMOC. We considered the role of temperature and salinity and how these tracers are affected by changes in surface flux and transport. The values of the different terms integrated over 500 years are summarized in Tables 1 and 2. All terms are of importance in understanding the density balance. It is therefore the difference in magnitude between them that results in a positive and negative balance, in WIS2-CTRL and NIS2-CTRL, respectively. In NIS2, without glacier melting, the leading recovery term (+32%) is the transport of salinity anomalies ($-V_{\mathrm{ctrl}}\,\Delta S$) from the tropics, which is associated to an increase in the Atlantic-Pacific and Antarctic atmospheric export of moisture. Thus, the Atlantic basin becomes more evaporative than in the CTRL simulation. The northward gyre transport of saline water increases salinity at the convection sites and allows the AMOC to recover. The role played by the northward advection of salinity anomalies was noted by Latif et al. (2000) in scenario simulations. That said, Latif et al. related salinity anomalies to a permanent El-Nino in their model, this is not the case here.

The anomalies in sea-ice melting (Ice in Table 1) is another major contributor (+15%) to AMOC recovery. A decrease of sea-ice transport in the convection sites, associated with sea-ice cover reduction in the Arctic, explain this modification in sea-ice forcing. The major processes at the origin of the weakening of the AMOC during NIS2 is the short wave heat flux change (–30%). Two other important terms are the non linear transport of salinity ($-\Delta V\,\Delta S$, –18%) and the anomalous transport of salinity ($-\Delta V\,S_{\mathrm{ctrl}}$, –17%). The recovery mechanisms proposed here combine various processes, several of which have been hypothesized in previous studies. Here we clarify the magnitude of each of them in the IPSL-CM4.

The balance in WIS2 is affected by several feedbacks and, in order to isolate them, we adapted the notion of climate sensitivity to the AMOC system. This allowed us to quantify the feedback factors of different processes, thus clarifying the existence and magnitude of AMOC coupled feedbacks via a comparison of WIS2 and NIS2 (Table 3). In agreement with Stommel (1961), the main feedbacks are related to salinity transport, which is a positive feedback, and heat transport, which is a negative feedback. Moreover, we have also shown the importance of two other feedbacks:

- The ocean–atmosphere heat flux counteracts the negative heat transport feedback and appears to be the second strongest positive feedback, after the feedback $\lambda_{\Delta V S_{\mathrm{ctrl}}}$ associated with the transport of salinity by the anomalous velocity field.
- The relative cooling in northern high latitudes, due to a reduction in the AMOC, leads to an increase of sea-ice amount in the Arctic, which increases sea-ice export towards the convection sites, and weakens the AMOC. This mechanism dominates the local brine rejection at the convection sites due to surface cooling. Thus, the global feedback related to interaction between AMOC and sea-ice is a positive feedback, but of second order magnitude.

We show that the sum of all these feedbacks is positive. This is due to the dominance of positive feedbacks, notably the heat flux feedback that strongly attenuates the damping effect of the heat transport feedback. The resulting feedback factor shows that the perturbation of the AMOC by land-ice melting is amplified by a factor 2.5.

This study established that the integrated effect of the land-ice melting should be incorporated in CGCM in order to take account of their effect on future climate. In this study, the amount of freshwater (due to Greenland melting)

brings a stabilized input of 0.13 Sv after 200 years. The present experiments can be considered as sensitivity experiments, showing that for IPSL-CM4, under global warming conditions, a difference of 0.13 Sv can cause the AMOC to shutdown. Rahmstorf et al. (2005) have recently shown with an inter-comparison study of intermediate complexity models that the hysteresis loop of the AMOC against freshwater forcing is around 0.2 Sv. Consequently the AMOC in WIS2 will not necessarily recover after the end of the Greenland melting. This possibility of non-linear behavior should be further investigated.

These results can be affected by biases in the IPSL-CM4 model. For instance, the weakness of the AMOC in CTRL may limit the strength of transport feedbacks. The modeling of land-ice melting can also be improved, thanks to the coupling with an ice-sheet model for instance. Further studies with other models would also help to better constrain the impact of land-ice melting on the AMOC on multi-century scale. The lack of direct observations of the AMOC and of land-ice melting remains an issue to validate CGCMs. The ongoing effort has to be pursued in order to provide reliable projections about possible changes of the AMOC. Applying the methodology we developed here to multi-model ensemble like the ''water hosing'' experiments (Stouffer et al. 2006) will be of great interest to analyze feedback differences between models.

Acknowledgments We thank Alessandro Tagliabue who kindly proofread the manuscript. We gratefully acknowledge the constructive comments from Ron Stouffer and two other anonymous reviewers. The coupled simulations were carried out on the NEC SX6 of the Centre de Calcul de Recherche et Technologie (CCRT). This work was supported by the Commissariat a l'Energie Atomique (CEA), and the Centre National de la Recherche Scientifique (CNRS). It is a contribution to the European project ENSEMBLES (Project No GOCE-CT-2003-505539).

References

Cubasch U et al (2001) Third assessment report of climate change, chap 8. Intergovernmental panel on climate change. Cambridge University Press, Cambridge, p 572

Delworth T, Manabe S, Stouffer R (1993) Interdecadal variations of the thermohaline circulation in a coupled Ocean–Atmosphere model. J Climate 6:1993–2011

Fichefet T, Poncin C, Goosse H, Huybrechts P, Jansses I, Treut HL (2003) Implication of changes in freshwater flux from the Greenland ice sheet for the climate of the 21st century. Geophys Res Lett 30:1911

Forster P, Taylor K (2006) Climate forcings and climate sensitivities diagnosed from coupled climate model integrations. J Climate 19:6181–6194

Ganachaud A, Wunsch C (2000) Improved estimates of global ocean circulation, heat transport and mixing from hydrographic data. Nature 407:453–457

Gregory JM et al (2005) A model intercomparison of changes in the Atlantic thermohaline circulation in response to increasing atmospheric CO_2 concentration. Geophys Res Lett 32:L12703

Gregory J, Saenko O, Weaver A (2003) The role of the Atlantic freshwater balance in the hysteresis of the meridional overturning circulation. Clim Dyn 21:707–717

Guilyardi E (2006) El Nino-mean state-seasonal cycle interactions in a multi-model ensemble. Clim Dyn 26:329–348

Hansen J, Lacis A, Rind D, Russell G, Stone P, Fung I, Ruedy R, Lerner J (1984) Climate sensitivity: analysis of feedback mechanisms. Clim Process Clim Sensitivity 29:130–163

Hu A, Meehl G, Washington W, Dai A (2004) Response of the Atlantic thermohaline circulation to increased atmospheric CO_2 in a coupled model. J Climate 17:4267–4279

Hughes T, Weaver A (1994) Multiple equilibria of an asymetric 2-basin ocean model. J Phys Oceanogr 24:619–637

Jungclaus J, Haak H, Esch M, Roeckner E, Marotzke J (2006) Will Greenland melting halt the thermohaline circulation? Geophys Res Let 33: Art. No. L17708

Latif M, Roeckner E, Mikolajewicz U, Voss R (2000) Tropical stabilisation of the thermohaline circulation in a greenhouse warming simulation. J Clim 13:1809–1813

Marti O, et al. (2005) The new IPSL climate system model: IPSL-CM4. Note du pôle de modélisation n 26. ISSN 1288-1619, 88 pp, http://www.dods.ipsl.jussieu.fr/omamce/IPSLCM4/DocIPSLCM4/

Meehl GA, Washington WM, Arblaster JM, Bettge TW, Strand WG (2000) Anthropogenic forcing and decadal climate variability in sensitivity experiments of twentieth- and twenty-first-century climate. J Clim 13:3728–3744

Parizek BR, Alley RB (2004) Implications of increased Greenland surface melt under globalwarming scenarios: ice-sheet simulations. Quat Sci Rev 23:1013–1027

Overpeck J, Otto-Bliesner B, Miller G, Muhs D, Alley R, Kiehl J (2006) Paleoclimatic evidence for future ice-sheet instability and rapid sea-level rise. Science 311:1747–1750

Rahmstorf S (1996) On the freshwater forcing and the transport of the Atlantic thermohaline circulation. Clim Dyn 12:799–811

Rahmstorf S et al (2005) Thermohaline circulation hysteresis: a model intercomparison. Geophys Res Let 32: Art. No. L23605

Ridley J, Huybrechts P, Gregory J, Lowe J (2005) Elimination of the Greenland ice sheet in a high CO_2 climate. J Climate 18:3409–3427

Stommel H (1961) Thermohaline convection with two stable regimes of flow. Tellus 13:224–230

Stouffer R et al (2006) Investigating the causes of the response of the thermohaline circulation to past and future climate changes. J Climate 19:1365–1387

Stouffer R, Manabe S (1999) Response of a coupled ocean–atmosphere model to increasing atmospheric carbon dioxide: sensitivity to the rate of increase. J Climate 12:2224–2237

Straub D (1996) An inconsistency between two classical models of the ocean buoyancy driven circulation. Tellus A 48:477–481

Swingedouw D, Braconnot P, Marti O (2006) Sensitivity of the Atlantic Meridional Overturning Circulation to the melting from Northern glaciers in climate change experiments. Geophys Res Lett 33:L07711

Swingedouw D, Braconnot P, Delecluse P, Guilyardi E, Marti O (2007) The impact of global freshwater forcing on the thermohaline circulation: adjustment of North Atlantic convection sites in a CGCM. Clim Dyn 28:291–305

Thorpe R, Gregory J, Johns T, Wood R, Mitchell J (2001) Mechanisms determining the atlantic thermohaline circulation response to greenhouse gas forcing in a non-flux-adjusted coupled climate model. J Climate pp 3102–3116

Vellinga M, Wood R, Gregory J (2002) Processes governing the recovery of a perturbed thermohaline circulation in HadCM3. J Climate 15:764–780

Voss R, Mikolajewicz U (2001) Long-term climate changes due to increased CO_2 concentration in the coupled atmosphere–ocean general circulation model ECHAM3/LSG. Clim Dyn 17

Wood RA, Keen AB, Mitchell JFB, Gregory JM (1999) Changing spatial structure of the thermohaline circulation in response to atmospheric CO_2 forcing in a climate model. Nature 399:572–575

Yang J, Neelin J (1993) Sea-ice interaction with the thermohaline circulation. Geophys Res Lett 20:217–220